CHAPTER 3

EXTENSION OF THE PROPOSED LTC TO THE FIELD WEAKENING RANGE

3.1 Introduction

In the previous chapter, a linear torque control (LTC) strategy for fully utilizing the reluctance torque of an IPMSM has been proposed. Based on the proposed linear torque control strategy, the constant torque limit speed range can be extended considerably wider than that of $i_{ds} = 0$ control strategy. For example, Fig. 2.1(a) shows the maximum torque limit to speed curves of $i_{ds} = 0$ control and the LTC by using the IPMSM parameters of [13]. One can see that the constant torque limit region has been extended to 197% of that of $i_{ds} = 0$ control. However, when the motor speed is greater than the base speed that is commonly called field weakening region, the maximum torque capability of the IPMSM is decreased with the increase of the motor speed. But there is still considerable torque capability available in the higher speed region. Thus, to fully exploit the available torque capability when the motor speed is higher than the base speed becomes the major motivation of this chapter.

In this chapter, the extension of the operation range to the field weakening range by using the proposed LTC such that the IPMSM drive can be operated over much wider speed range will be presented. The theoretical basis of the proposed field weakening control is proposed and the corresponding analytical forms are derived for the first time in this chapter. The whole operational regions of an IPMSM are divided into three regions according to the motor speed. They are the constant torque limit region (Region I), the partial field weakening

region (Region II), and the full field weakening region (Region III). However, only two control modes, namely the constant torque limit control mode and the field weakening control mode, are required. A control mode detector is proposed to choose the correct control mode efficiently according to the motor speed and the demanded torque. In addition, to fully use the maximum torque capability in the field weakening region, a variable torque limiter is also proposed to simplify the complexity of the control algorithm. Finally, the proposed control is also implemented fully digitally by using a fixed point DSP TMS320F240 to simplify the hardware circuits and some experimental results are given to verify the effectiveness of the extension of the proposed LTC to the field weakening range.

3.2 The Proposed Field Weakening Control

As described in the previous chapter that the maximum attainable speed to maintain the maximum torque capability is ω_{rm}. The operation speed range below ω_{rm} is usually called constant torque limit operation region. On the other hand, if one wishes the IPMSM to run at a speed greater than ω_{rm}, then the corresponding maximum attainable torque should be decreased. In other words, the IPMSM is now operated in the field weakening region. Therefore the corresponding torque control strategy should be further investigated. One can follow from (2.6), (2.7), and (2.22) to obtain the corresponding voltage limit equation as:

$$(R_S\, i_{ds} - \omega_r L_q\, i_{qs})^2 + (R_S\, i_{qs} + \omega_r L_d\, i_{ds} + \omega_r \lambda_{mf})^2 = V_{sm}^2 \tag{3.1}$$

Fig. 3.1 illustrates a curve AIO as the trajectory of (2.20) as well as the current limit curve and some voltage limit curves on the i_{ds}-i_{qs} plane. In Fig. 3.1 there are five voltage limit curves corresponding to five speeds ω_{rm}, ω_{r1}, ω_{rC}, ω_{r2}, and ω_{rE} where $\omega_{rm} < \omega_{r1} < \omega_{rC} <$

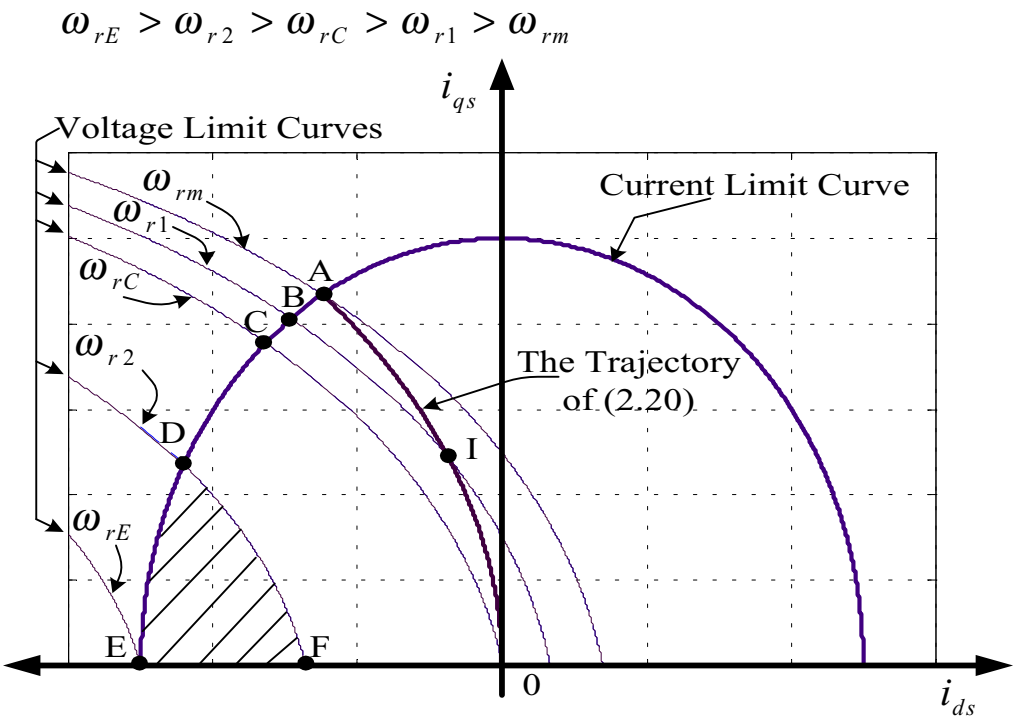

Fig. 3.1. The trajectories of (2.20), the current limit curve, and five voltage limit curves on i_{ds}-i_{qs} plane for a sample IPMSM.

$\omega_{r2} < \omega_{rE}$. One can see when $\omega_r = \omega_{rm}$ the voltage limit curve intersects with trajectory AIO at point A lying on the current limit curve. Just as described in the previous chapter, the trajectory AIO is within the area of current limit and voltage limit constraints. When $\omega_r = \omega_{rC}$ the voltage limit curve intersects with current limit curve at point C. Also it intersects with the trajectory AIO at the origin (0, 0). When $\omega_r = \omega_{rE}$ the voltage limit curve intersects with the current limit curve at point E. As will be explained later, ω_{rE} is the theoretical maximum operation speed under both current constraint (2.21) and voltage constraint (2.22).

Following from the above results, one can divide the speed range into three operation regions for the proposed linear torque controlled IPMSM drive as follows:

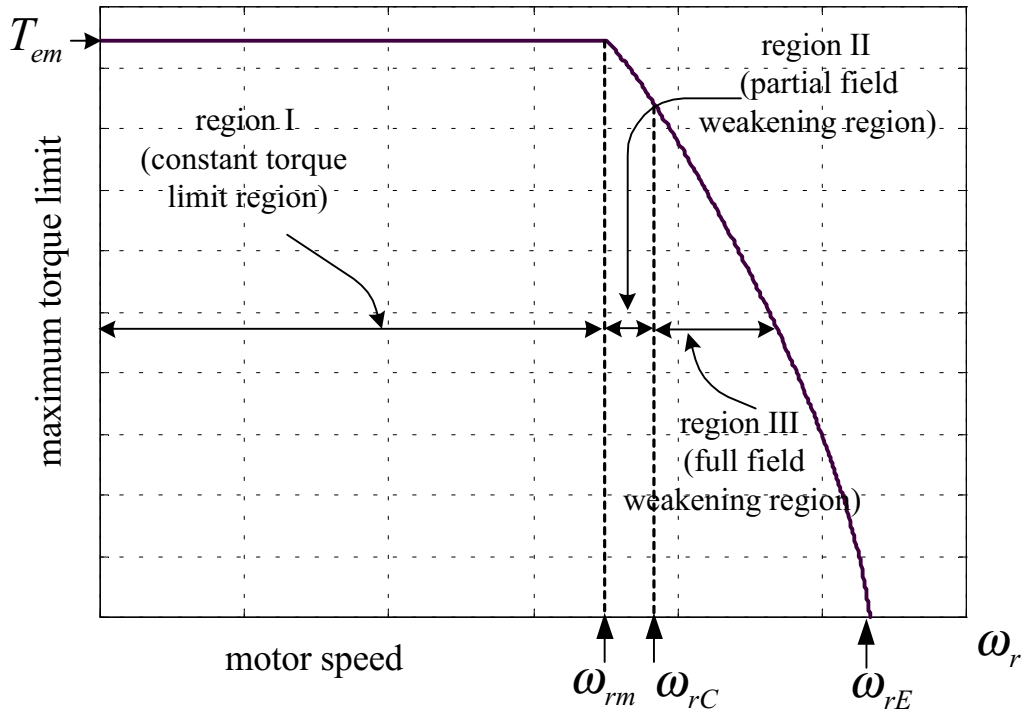

Fig. 3.2. Illustration of a maximum torque limit to speed curve and three speed regions for a prototype IPMSM designed in [67].

Region I. Constant Torque Limit Region ($\omega_r \le \omega_{rm}$)

As $\omega_r \le \omega_{rm}$, the previously proposed linear torque control (LTC) strategy is used to generate the d-axis and q-axis current commands (i_{ds}^* and i_{qs}^*). For clarity, Fig. 3.2 also gives the maximum torque limit to speed curve for an IPMSM in the whole speed range. The Region I as shown in Fig. 3.2 is just the constant torque limit region discussed previously.

Region II. Partial Field Weakening Region ($\omega_{rm} < \omega_r \le \omega_{rC}$)

From Fig. 3.1 one can see that when $\omega_r = \omega_{r1}$, where $\omega_{rm} < \omega_{r1} \le \omega_{rC}$, the voltage limit curve intersects with the trajectory AIO at point I. If the desired current command magnitude

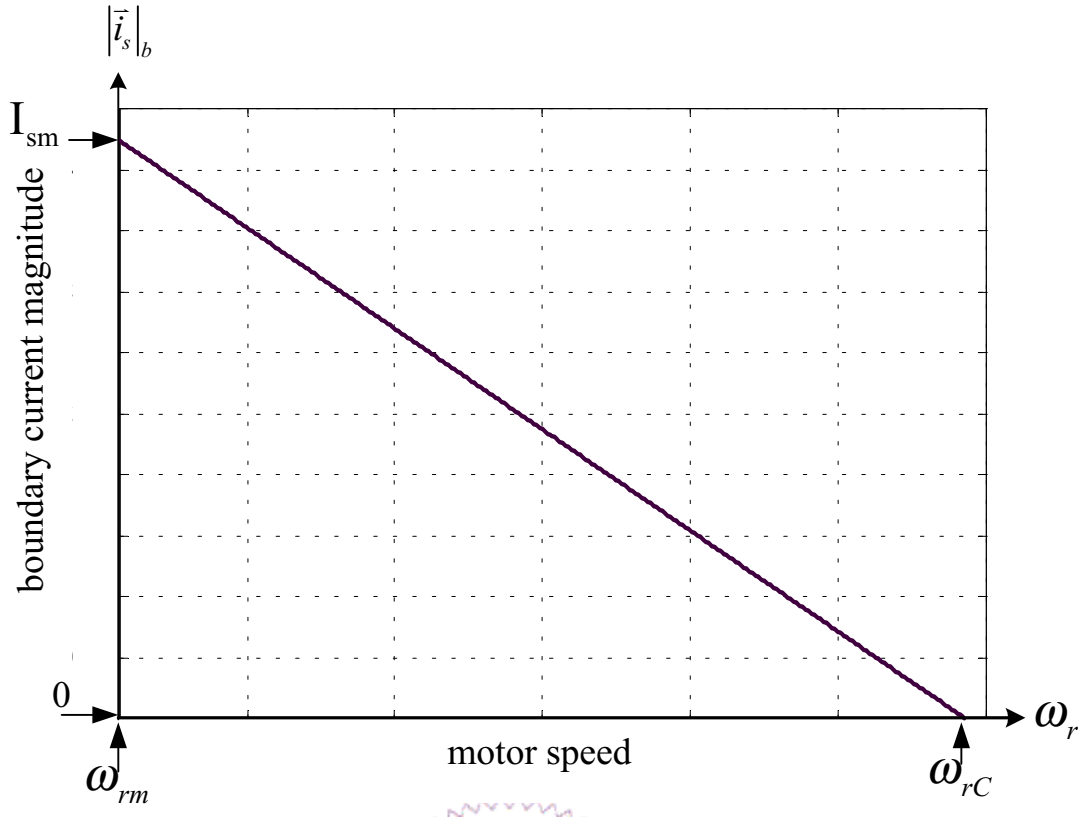

Fig. 3.3. Graphical illustration of the boundary current magnitude to motor speed curve for $\omega_{rm} \le \omega_r \le \omega_{rC}$

$|\vec{i}_s^*|$ corresponding to a particular load torque intersects the trajectory AIO at a point located below point I, then the LTC strategy can still be applied. On the other hand, if the desired $|\vec{i}_s^*|$ intersects the trajectory AIO at a point that is above point I, a different torque control strategy, called the field weakening control, should be applied. Since in this region, for each $\omega_r \in (\omega_{rm}, \omega_{rC}]$, depending on the magnitude of the loading torque, either the constant torque limit control or the field weakening control is chosen. Hence, Region II is called the partial field weakening region. Furthermore, from the implementation point of view, one can define the boundary current magnitude as

$$\left|\vec{i}_s\right|_b \triangleq \sqrt{i_{dsb}^2 + i_{qsb}^2} \tag{3.2}$$

where (i_{dsb}, i_{qsb}) is the intersecting point of the voltage limit curve and the trajectory AIO for each $\omega_r \in (\omega_{rm}, \omega_{rC}]$. When the $\left|\vec{i}_s^{\,*}\right| > \left|\vec{i}_s\right|_b$, then a field weakening control should be used, otherwise the constant torque limit control is adopted. The corresponding boundary current magnitude to speed curve is shown in Fig. 3.3 for illustration. From Fig. 3.3 one can see when $\omega_r = \omega_{rC}$ the corresponding boundary current magnitude is zero. Therefore ω_{rC} can be determined from (3.1) by letting (i_{ds}, i_{qs})=(0, 0):

$$\omega_{rC} = \frac{\mathrm{V_{sm}}}{\lambda_{\mathrm{mf}}} \tag{3.3}$$

Region III. Full Field Weakening Region ($\omega_{rC} < \omega_r \le \omega_{rE}$)

When the motor speed ω_r is greater than ω_{rC}, as reference to Fig. 3.1, the corresponding voltage limit curve is located to the left-hand side of the voltage limit curve corresponding to $\omega_r = \omega_{rC}$. For example the voltage limit curve at $\omega_r = \omega_{r2}$, as shown in Fig. 3.1, intersects with the current limit curve at point D. The operable area satisfying both current limit and voltage limit constraints is the hatched area DEF as denoted in Fig. 3.1. One can observe that the operable area satisfying both current limit and voltage limit constraints is getting smaller as the motor speed ω_r is increased. Finally while the motor speed reaches an extreme speed ω_{rE}, the operable area becomes zero. This extreme motor speed ω_{rE} is the theoretical maximum operation speed for the motor drive and can be determined from (3.1) by letting (i_{ds}, i_{qs})=($-\mathrm{I_{sm}}$, 0):

$$\omega_{rE} = \frac{\sqrt{V_{sm}^2 - (R_s I_{sm})^2}}{\lambda_{mf} - L_d I_{sm}} \tag{3.4}$$

where $\lambda_{mf} - L_d I_{sm} > 0$ as far as the parameters of the IPMSM are concerned. For reference, in Fig. 3.2 also shows the full field weakening region (Region III). In summary, the proposed linear torque control divides the entire operation range into three regions. The first region, $0 \le \omega_r \le \omega_{rm}$, is the constant torque limit region. For $\omega_r \in (\omega_{rm}, \omega_{rC}]$, it is called the partial field weakening region, and for $\omega_r \in (\omega_{rC}, \omega_{rE}]$, it is called the full field weakening region. The remaining question is to find the field wakening control for region III and part of region II. Since for a given loading, the corresponding torque command T_e^*=0.75P$[\lambda_{mf} + (L_d - L_q)$ $i_{ds}^*]i_{qs}^*$. Hence one can get

$$i_{qs}^* = \frac{K_t(\pm|\vec{i}_s^*|)}{0.75p\left[\lambda_{mf} + (L_d - L_q)i_{ds}^*\right]} \tag{3.5}$$

where K_t is the optimal torque constant corresponding to the LTC strategy. Also, under field weakening control, the motor currents are limited by the voltage constraint of (3.1). Hence, by substituting (3.5) into (3.1), one can obtain the desired i_{ds}^* from the following equation:

$$\{R_s i_{ds}^* - \omega_r L_q \frac{K_t(\pm|\vec{i}_s^*|)}{0.75p[\lambda_{mf} + (L_d - L_q)i_{ds}^*]}\}^2 + \{\frac{R_s K_t(\pm|\vec{i}_s^*|)}{0.75p[\lambda_{mf} + (L_d - L_q)i_{ds}^*]} + \omega_r(L_d i_{ds}^* + \lambda_{mf})\}^2 = V_{sm}^2 \tag{3.6}$$

The corresponding i_{qs}^* can then be obtained from (3.5) directly.

3.3 Implementation of the Proposed Control Strategy

Fig. 3.4 illustrates the block diagram of the speed control system implemented by the proposed LTC strategy. The line current magnitude command $\pm\left|\vec{i}_s^{\,*}\right|$ is generated from the speed error $(\omega_r^* - \omega_r)$ through a proportional integral (PI) speed controller and a torque limiter. In the torque limiter block for $\omega_r \le \omega_{rm}$, the maximum line current magnitude $\left|\vec{i}_s\right|_{\max}$ is limited at the maximum line current magnitude $\mathrm{I_{sm}}$. On the other hand when $\omega_r > \omega_{rm}$, the maximum line current magnitude is smaller than $\mathrm{I_{sm}}$ and varies with motor speed ω_r. In fact, the function of the torque limiter block in Fig. 3.4 is the extension of the line current magnitude command limiter as shown in Fig. 2.3 to cover the full operation speed range.

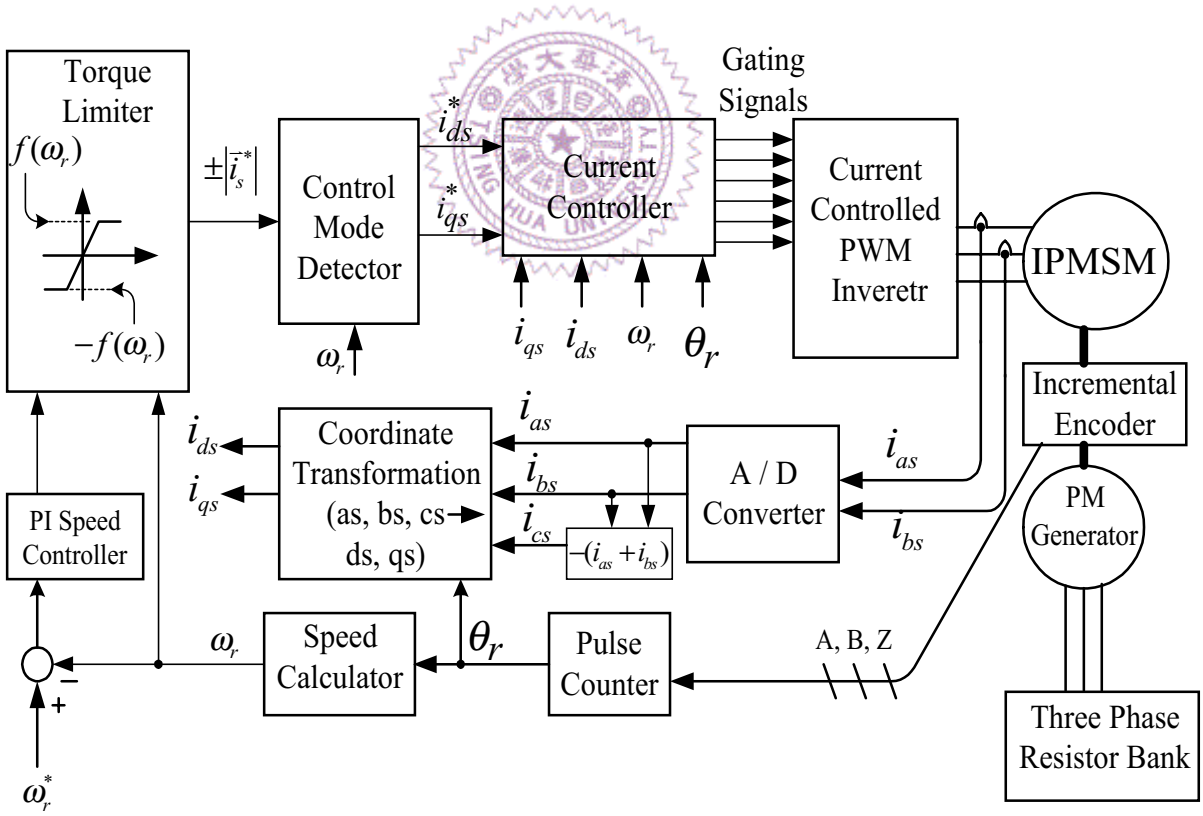

Fig. 3.4. Block diagram of the proposed speed control system for an IPMSM drive.

For each $\omega_r > \omega_{rm}$, the d- and q-axis currents of the maximum attainable torque, named $i_{ds\_\max T}$ and $i_{qs\_\max T}$ respectively, is the intersecting point of the current limit curve and the voltage limit curve. To obtain $i_{ds\_\max T}$ and $i_{qs\_\max T}$ (where $i_{qs\_\max T} = \sqrt{\mathrm{I}_{\mathrm{sm}}^2 - i_{ds\_\max T}^{*\,2}}$), one can substitute $i_{qs} = \sqrt{\mathrm{I}_{\mathrm{sm}}^2 - i_{ds\_\max T}^{*\,2}}$ into (3.1) to yield:

$$\begin{aligned}&(\mathrm{R_S}\, i_{ds\_\max T} - \omega_r \mathrm{L_q} \sqrt{\mathrm{I}_{\mathrm{sm}}^2 - i_{ds\_\max T}^{2}})^2 + \\ &(\mathrm{R_S} \sqrt{\mathrm{I}_{\mathrm{sm}}^2 - i_{ds\_\max T}^{2}} + \omega_r \mathrm{L_d}\, i_{ds\_\max T} + \omega_r \lambda_{\mathrm{mf}})^2 = \mathrm{V}_{\mathrm{sm}}^2\end{aligned} \tag{3.7}$$

Following from (3.7), one can obtain $i_{ds\_\max T}$ and $i_{qs\_\max T}$. Thus the maximum attainable torque $T_{e\_\max T}$ for $\omega_r > \omega_{rm}$ is

$$T_{e\_\max T}\Big|_{\omega_r} = 0.75\mathrm{p}\left[\, \lambda_{\mathrm{mf}} + (\mathrm{L_d} - \mathrm{L_q})\, i_{ds\_\max T} \,\right] i_{qs\_\max T} \tag{3.8}$$

In order to preserve the linear torque control property, the line current magnitude limit in the torque limiter block can be implemented as:

$$\left|\vec{i}_s\right|_{\max} \triangleq f(\omega_r) = \begin{cases} \mathrm{I}_{\mathrm{sm}}, & 0 \le \omega_r \le \omega_{rm} \\ \dfrac{T_{e\_\max T}}{K_t}, & \omega_{rm} < \omega_r \le \omega_{rE} \end{cases} \tag{3.9}$$

As an illustration, a complete line current magnitude limit, namely $f(\omega_r)$, for three operation regions is shown in Fig. 3.5. Comparing Fig. 3.5 with Fig. 3.2, it is seen that both figures are basically similar in shape.

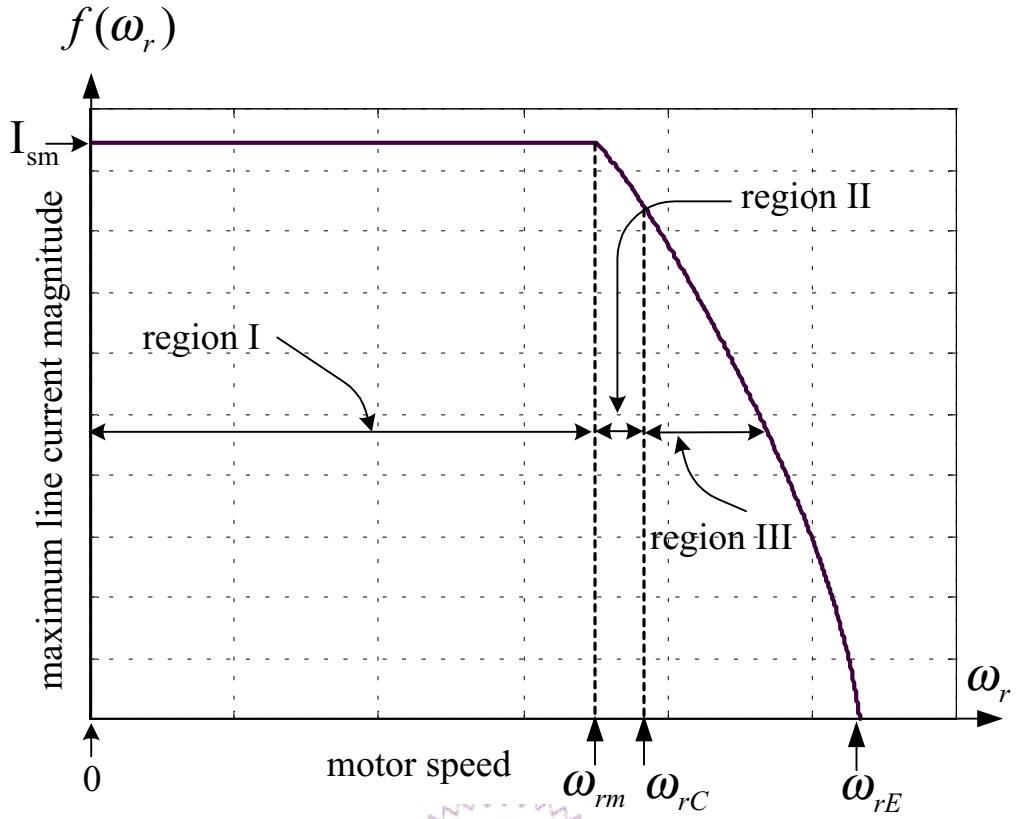

Fig. 3.5. Illustration of the maximum line current magnitude to motor speed curve for $0 \le \omega_r \le \omega_{rE}$

In fact, it is the natural result of the proposed linear torque control where $T_e^* (= \pm K_t \left| i_s^* \right|)$ is proportional to $\left| \vec{i}_s^{\,*} \right|$. During acceleration or deceleration, in order to achieve fast performance, the maximum torque capability corresponding to the motor speed ω_r is fully utilized. Once the command speed is reached, then the resulting torque will settle down to the corresponding load torque. At this equilibrium point, the corresponding i_{ds}^* and i_{qs}^* have been given in the previous section. From the above description, one can see that the proposed torque limiter with variable limits, in fact, defines a special transient trajectory on the i_{ds}^*-i_{qs}^* plane to achieve fastest response.

Once the line current magnitude command $\pm\left|\vec{i}_s^{\,*}\right|$ is available, the corresponding i_{ds}^* and i_{qs}^* can be decided by the control mode detector block in Fig. 3.4. The function of the control mode detector block in Fig. 3.4 is to calculate the desired d- and q-axis current commands according to the demanded torque and the motor speed over the full speed range. One can check that there doesn't exist a control mode detector block in Fig. 2.3 where the corresponding operation speed is within the constant torque limit speed range. The detailed description of the control mode detector block is addressed as follows. In addition, a flowchart is shown in Fig. 3.6 as a reference.

a) As shown in Fig. 3.6, firstly if the motor speed is below the base speed ($\omega_r < \omega_{rm}$), the drive is operated in Region I. Hence, from (2.25) and (2.26) one can use two second order polynomials to approximate the corresponding i_{ds}^* and i_{qs}^*, respectively as follows

$$i_{ds}^* = \mathrm{k1}\left|\vec{i}_s^{\,*}\right|^2 + \mathrm{k2}\left|\vec{i}_s^{\,*}\right| + \mathrm{k3} \tag{3.10}$$

$$i_{qs}^* = \mathrm{k4}\left|\vec{i}_s^{\,*}\right|^2 + \mathrm{k5}\left|\vec{i}_s^{\,*}\right| + \mathrm{k6} \tag{3.11}$$

where k1 to k6 are all real constants. Therefore for a given line current magnitude command $\pm\left|\vec{i}_s^{\,*}\right|$, the corresponding i_{ds}^* and i_{qs}^* can be readily calculated from (3.10) and (3.11) respectively.

b) If the motor speed exceeds base speed ($\omega_r \geq \omega_{rm}$), the process runs into another decision block to decide whether the drive is in Region III (the full field weakening region) or in Region II (the partial field weakening region). If $\omega_r < \omega_{rC}$, the drive is

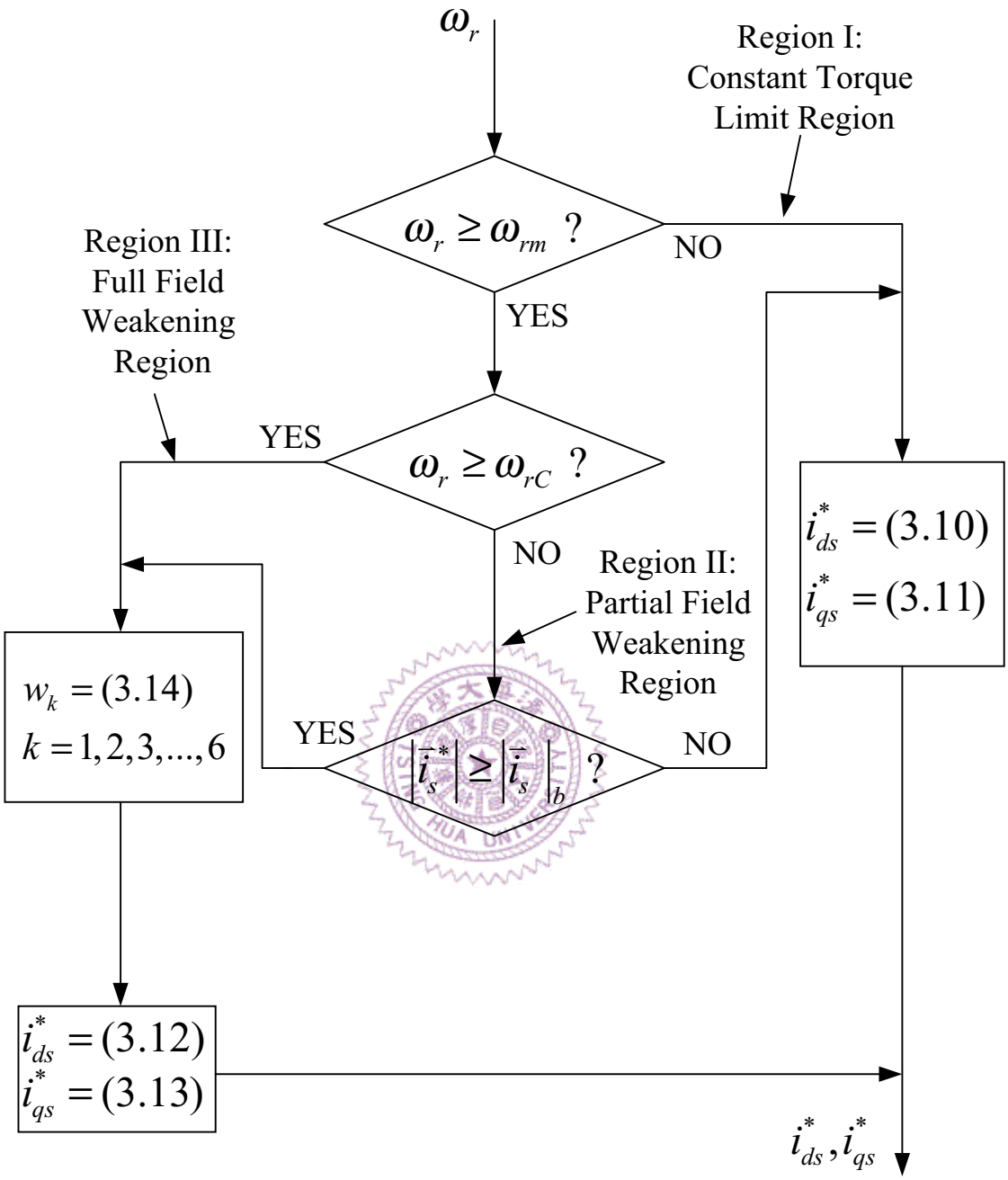

Fig. 3.6. The flowchart of the control mode detector corresponding to Fig. 3.4.

in the partial field weakening region; otherwise for $\omega_r \geq \omega_{rC}$, the process can directly go to the full field weakening region.

c) In the full field weakening region, following from (3.5) and (3.6) one can use two more second order polynomials to approximate the corresponding i_{ds}^* and i_{qs}^*, respectively as follows:

$$i_{ds}^* = w_1 \left|\vec{i}_s^*\right|^2 + w_2 \left|\vec{i}_s^*\right| + w_3 \tag{3.12}$$

$$i_{qs}^* = w_4 \left|\vec{i}_s^*\right|^2 + w_5 \left|\vec{i}_s^*\right| + w_6 \tag{3.13}$$

where w_1 to w_6 are real coefficients. Because coefficients w_i , $i = 1\text{-}6$, in (3.12) and (3.13) are varied with $\omega_r \in (\omega_{rm}, \omega_{rE}]$, they can be again formulated as functions of ω_r in the entire field weakening range. Thus, let

$$w_k = a_{k1}\omega_r^2 + a_{k2}\omega_r + a_{k3} \ , k = 1,2,3,...,6 \tag{3.14}$$

where a_{kj} $,k = 1,2,3,...,6,\ j = 1,2,3$ are all real constants. From actual experiments, it is found that a second order polynomial approximation is accurate enough for the test. Thus, the numerical calculations can be simplified greatly. Furthermore, due to the fast computational speed and the available large amount of memory of a modern digital signal processor, the above complicated calculations can be easily implemented with satisfactory accuracy and can be processed in real time. Therefore the six coefficients of (3.14) are first calculated. Then i_{ds}^* and i_{qs}^* can be readily determined by (3.12) and (3.13) respectively.

d) In the partial field weakening region, the motor speed is between ω_{rm} and ω_{rC}. For each $\omega_r \in (\omega_{rm}, \omega_{rC}]$, if the line current magnitude command $\left|\vec{i}_s^*\right|$ is less than the

boundary line current magnitude $\left|\bar{i}_s\right|_b$, then the process jumps to the constant torque limit region block; otherwise, the process jumps to the full field weakening region block.

3.4 Experimental Results

In order to verify the feasibility of the proposed control strategy, a DSP based vector controlled IPMSM drive has been built. The system block diagram has already been shown in Fig. 3.4. In Fig. 3.4, the functions of PI speed controller, torque limiter, control mode detector, current controller, coordinate transformation, A/D converter, speed calculator, and pulse counter are all implemented within a fixed-point DSP TMS320F240. The sampling time period for the speed controller is chosen to be 1 msec and the sampling time period of the current controller is chosen to be 0.1 msec. The features of the torque limiter and the control mode detector have been detailed described in Section 3.3. The tested IPMSM, a prototype designed in [67], has the parameters of motor D as shown in Table 2.1. Thus, the corresponding ω_{rm} is 3500 rpm being determined from (2.24), the ω_{rC} from (3.3) is 3790 rpm, and the d- and q-axis boundary currents (i_{dsm} and i_{qsm}) according to (2.23) are –12.4 (A) and 21.7 (A) respectively. Since the remaining parts of Fig. 3.4 are quite typical and they will not be explained further.

Three experimental results will be illustrated to show the characteristics of the proposed integrated linear torque control strategy. To demonstrate the smooth transitions between the constant torque limit region operation and the field weakening region operation, first consider the case of applying a step command of ω_r^*=3650 rpm to the tested IPMSM drive starting from rest at t=0 sec and with lighter load such that the motor is settled down to the

constant torque limit control. Fig. 3.7 shows the d- and q-axis current responses, speed response, and the bottom trace shows the region status indicating the transition between the constant torque limit control mode and the field weakening control mode. As can be observed from Fig. 3.7, when the motor is accelerating with its speed below $\omega_r = \omega_{rm}$ =3500 rpm, the motor is operated in Region I and the responses of i_{ds} and i_{qs} keep approximately constant at i_{dsm} and i_{qsm} respectively. Therefore the bottom trace of Fig. 3.7 shows that the region status is at low level (the constant torque limit control mode). As soon as ω_r is greater than ω_{rm} =3500 rpm,

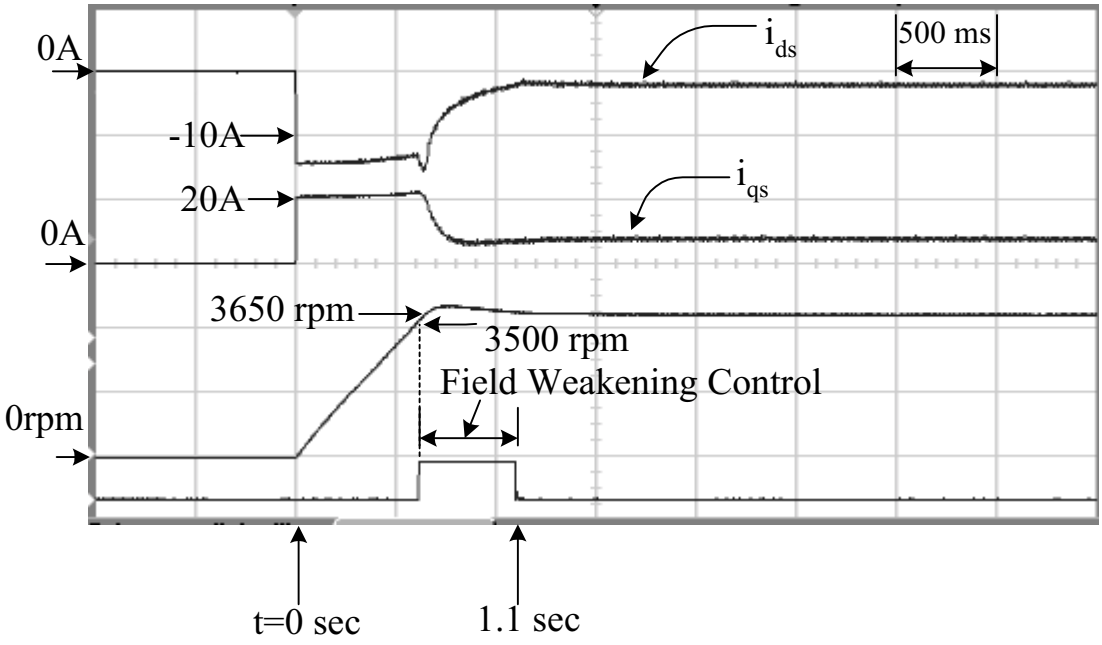

Fig. 3.7. Experimental results of i_{ds} , i_{qs} , and motor speed responses for the proposed control strategy in the partial field weakening region under lighter load.

the motor is then operated in Region II. The responses of i_{ds} and i_{qs} decrease with the increase of ω_r according to (3.9) until the motor speed ω_r is greater than the speed command ω_r^*=3650. Meanwhile, the region status at the bottom trace of Fig. 3.7 has changed from the low level (the constant torque limit control mode) to the high level (the field weakening control mode) at ω_r =3500 rpm. The field weakening control mode persists until about t=1.1 sec, then the motor speed reaches the steady state speed ω_r =3650 rpm and the bottom trace therefore shows a second transition from the high level to the low level again. It can be checked that the motor load torque (approximately 0.9 Nm at 3650 rpm) is less than $K_t \left|\vec{i}_s\right|_b$ at ω_r =3650 rpm. The second test condition is almost the same as the first one except that a heavier load is applied such that motor is settled down to the field weakening control region. Fig. 3.8 shows the d- and q-axis current responses, speed response, and the corresponding region status for a step speed command. One can see the region status in Fig. 3.8 that shows only one transition from the low level to the high level. It can also be checked that the load torque (approximately 3.9 Nm at 3650 rpm) is greater than $K_t \left|\vec{i}_s\right|_b$ at ω_r =3650 rpm. Thus the steady state operation mode is kept in the field weakening control mode. Finally, to demonstrate the operation mode in Region III, a step command of ω_r^*=4200 rpm which is greater than ω_{rC} =3790 rpm is applied to the IPMSM drive starting from rest at t=0 sec. Fig. 3.9 shows the corresponding d- and q-axis current responses, speed response, and the region status. As shown in Fig. 3.9, when the motor speed reaches $\omega_r = \omega_{rm}$ =3500 rpm the region status indicates a transition from low level to high level. When ω_r >3500 rpm, then i_{ds} and i_{qs} both start decreasing according to (3.9) until the motor speed ω_r is greater

than the speed command ω_r^*=4200 rpm at about t=0.8 sec. For t≥0.8 sec, the magnitude of i_{ds} is gradually decreased to the steady state magnitude of i_{ds}^* of (3.6) and the i_{qs} is gradually decreased to the corresponding steady state magnitude of (3.5). However, since the motor speed is greater than ω_{rC} =3790 rpm, the steady state operation mode is still kept in the field weakening control mode as can be observed from the region status of Fig. 3.9. The above experimental tests show that the proposed control strategy can indeed achieve much wider speed operation range and also can provide rather smooth transition between constant torque limit control mode and field weakening control mode for an IPMSM drive.

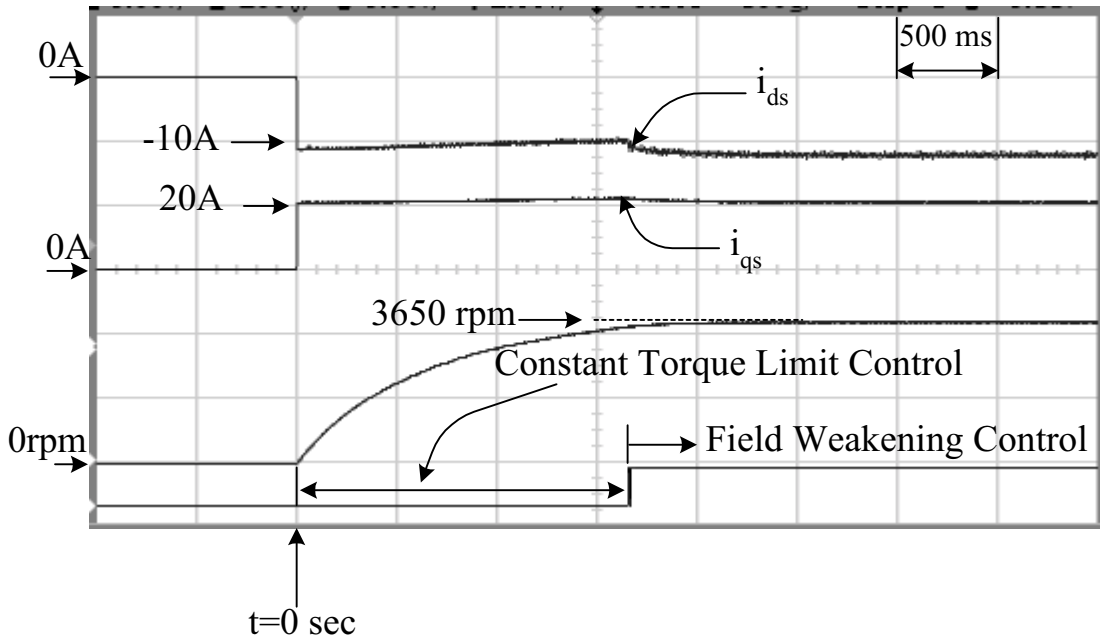

Fig. 3.8. Experimental results of i_{ds} , i_{qs} , and motor speed responses for the proposed control strategy in the partial field weakening region under heavier load.

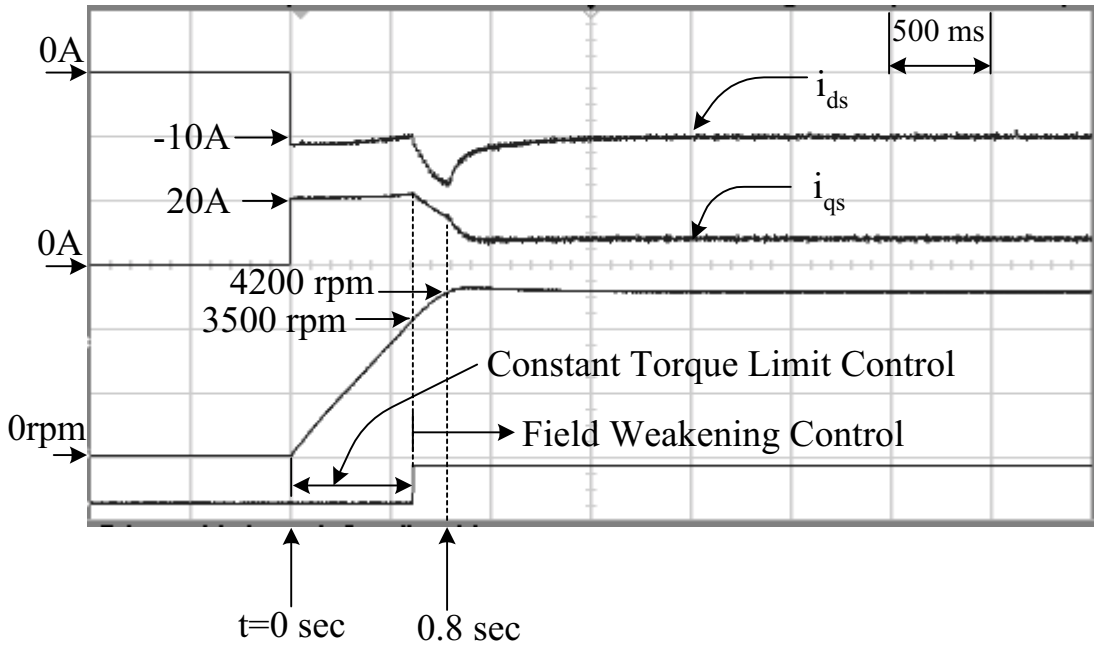

Fig. 3.9. Experimental results of i_{ds}, i_{qs}, and motor speed responses for the proposed control strategy in the full field weakening region.